Chemical Physics 366 (2009) 9–14

Contents lists available at ScienceDirect

Chemical Physics

journal homepage: www.elsevier.com/locate/chemphys

Isolated attosecond pulses from ionization gating of high-harmonic emission

Mark J. Abel *, Thomas Pfeifer, Phillip M. Nagel, Willem Boutu, M. Justine Bell, Colby P. Steiner, Daniel M. Neumark, Stephen R. Leone

Departments of Chemistry and Physics, University of California, Berkeley, CA 94720, United States
Chemical Sciences Division, Lawrence Berkeley National Laboratory, Berkeley, CA 94720, United States

ARTICLE INFO

Article history:
Received 21 May 2009
Accepted 15 September 2009
Available online 19 September 2009

Keywords:
Attosecond pulses
High-harmonic generation
Ultrafast optics
Carrier–envelope phase

ABSTRACT

Combining results from several techniques of attosecond spectroscopy, we show that ionization gating of high-harmonic emission on the leading edge of the driving pulse produces isolated attosecond pulses with a contrast ratio (the energy in the main pulse normalized to the energy in adjacent satellite pulses) $c = 3.3 \pm 0.2$. Half-cycle cutoff analysis confirms that harmonic generation proceeds in the ionization-gated regime. The attosecond pulse contrast is measured using the technique of carrier–envelope phase (CEP)-scanning, recently developed by our group, in which photoelectrons generated from Ne atoms by the harmonic pulse are streaked as a function of CEP. Streaking of photoelectrons as a function of attosecond time delay also confirms the isolated nature of the harmonic pulse, which is measured to have a duration of 430 ± 15 as, limited by the bandwidth of the reflective X-ray optics employed. The combined measurements imply that the experimental advantages of the ionization gating technique—tunable X-ray emission, relaxed sensitivity to the CEP and scalability to longer driver pulses—are also conferred on isolated attosecond pulse production.

Published by Elsevier B.V.

1. Introduction

The unprecedented temporal resolution offered by isolated attosecond pulses (IAPs) is opening a new field of physics and chemistry. Electronic motion in atoms [1], molecules, nanoparticles [2], and solids [3] can be probed in real time by using attosecond pulses overlapped with a phase-locked visible field. To achieve isolated attosecond pulses, soft X-ray light is generated in a process known as high-harmonic generation (HHG), in which a strong laser field ionizes atoms, accelerates the electrons in the continuum, and then accelerates the electrons back toward the ion where they can recombine, releasing their acquired kinetic energy as a photon. This process repeats every half-cycle of the driving laser field, so harmonic emission creates a train of attosecond pulses [4]. This quasi-classical 3-step model of HHG enables intuitive understanding and control over the harmonic generation process in the tunneling regime, ignoring the quantum mechanical interferences that determine electron dynamics in experiments with weaker driving laser fields [5–7].

Indeed, controlling the three steps of high-harmonic generation in strong laser fields offers opportunities to generate isolated attosecond pulses. For example, IAPs have been produced by varying the kinetic energy of the returning electron using the intensity variation of a few-cycle driving pulse [8], as well as by guiding the electrons' continuum motion by modulating the polarization of the driving pulse [9,10]. Two-color (heterodyne) schemes [11–15], in which the time-dependent intensity of the driving laser is modulated by mixing it with light of another color, appear quite promising but so far have not been directly proven to yield IAPs. Finally, combinations of the above methods [16,17] have been investigated theoretically and also show much promise.

These methods of IAP production are generally interpreted in terms of the microscopic response of individual atoms in the generation medium. In our group, we have developed a somewhat different approach, ionization gating, which offers the possibility of producing IAPs under less stringent conditions than other methods [18]. Moreover, it allows the attosecond pulse to be tuned over a large frequency range merely by varying the temporal offset between the extrema of the driving field and of the envelope, known as the carrier–envelope phase (CEP). Ionization gating has a macroscopic origin, relying on a sub-femtosecond loss of phase matching during the leading edge of the driving pulse [19]. In ionization gating, which is illustrated schematically in Fig. 1b, the intensity of the driving laser pulse is increased so that during the leading edge of the driving pulse the time-dependent ionization of the harmonic generation medium rises above the critical ionization level. At this plasma density, the negative dispersion due to free electrons cannot be compensated by the positive dispersion of the remaining

* Corresponding author. Address: Chemical Sciences Division, Lawrence Berkeley National Laboratory, Berkeley, CA 94720, United States.
E-mail addresses: abelm@berkeley.edu (M.J. Abel), srl@berkeley.edu (S.R. Leone).

0301-0104/$ - see front matter Published by Elsevier B.V.
doi:10.1016/j.chemphys.2009.09.016

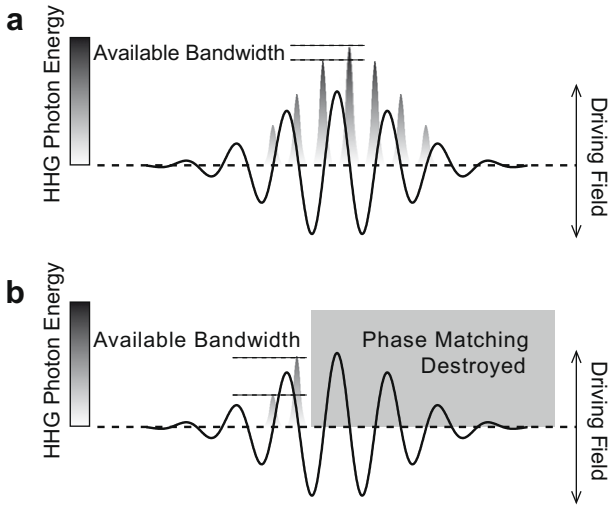

Fig. 1. *Traditional versus ionization-gated IAP production.* In early experiments with isolated attosecond pulses, the harmonic pulse corresponding to the strongest half-optical cycle of the visible driver pulse was isolated using a spectral filter. The available bandwidth is determined by the intensity difference between adjacent half-cycles near the peak of the driver pulse. In the ionization gating method, the intensity difference (and therefore the attosecond pulse bandwidth) can be much larger because of the rapid variation of the driver pulse intensity on the leading edge of the driver pulse.

neutral generation gas [20]. As a consequence, phase matching of the harmonic emission is no longer possible, thereby gating the harmonic emission on the leading edge of the driving laser pulse.

In the following sections, we first verify ionization gating conditions in the harmonic emission process using half-cycle cutoff (HCO) analysis [21], which allows the highest photon energies associated with individual bursts in the attosecond pulse train to be measured. As can be seen in Fig. 1a, for the non-gated case an attosecond pulse can be obtained at the very peak of the driving laser intensity envelope. In that case, the half-cycle cutoff energies will show a roughly Gaussian dependence on emission time, corresponding to the intensity envelope of the driving pulse. However, if the ionization gate closes before the peak of the pulse (Fig. 1b), the HCO energy depends nearly linearly on emission time. Previous HCO analyses [18,19] showed that broadband X-ray emission that is strongly indicative of IAPs could be obtained by the ionization gating method, but the temporal structure of the pulses was not measured. Here, we present a measurement of the contrast ratio of the IAPs, defined as the energy in the main IAP compared to the energy in any adjacent satellite pulses. Also, time-resolved optical streaking using a direct atomic ionization process is carried out to further confirm the isolated nature of the ionization-gated harmonic emission and to measure the duration of the attosecond pulse.

2. Experimental details

At the heart of the experimental apparatus (Fig. 2) is a 25 fs, 0.8 mJ Ti:Sapphire laser system operating at 3 kHz, with central wavelength 800 nm. The carrier–envelope phase is locked (0.3 rad RMS error) using a home-built feedback loop. Difference frequency mixing of the oscillator output in a periodically-poled lithium niobate (PPLN) crystal provides a second pulse train with zero carrier–envelope offset frequency to which the oscillator output is compared [22–24].

The laser output is focused into a capillary waveguide filled with neon gas at a pressure of 2 bar, where self-phase modulation broadens the spectrum and simultaneously shifts the central wavelength to about 730 nm [25–27]. The broadened capillary output is temporally compressed to ~7 fs by a set of chirped mirrors. The light transmitted through the first chirped mirror is sent to an f–2f interferometer to monitor and correct CEP drifts in the amplifier [28]. The chirped mirrors also precompensate for the dispersion caused by propagation through air and glass between the compressor and the HHG cell. The remainder of the compressed pulse is focused into the harmonic generation cell by a $f = 50$ cm mirror. The Rayleigh range is approximately 9 mm.

High-harmonic light is generated in a 2 mm path-length cell with 100 μm holes drilled for the laser entrance and exit. The pressure in the HHG cell is ~100 mbar. For the half-cycle cutoff measurements, the 730 nm light is filtered out of the combined beam path by two 200 nm thick zirconium filters and the remaining harmonic light is dispersed by a Si_3N_4 transmission grating with 100 nm period. The harmonic spectrum is recorded by a back-illuminated CCD camera with an acquisition time of 10 ms. Twenty harmonic spectra are recorded per CEP offset value.

For the CEP-scanning experiment [29], both the 730 nm and the X-ray pulses are reflected from a multilayer mirror composed of alternating layers of molybdenum and silicon. The mirror has a reflectivity band in the X-ray region centered at 93 eV with 4 eV FWHM and about 70% peak reflectivity, as well as ≃50% reflectivity across the entire visible and near-IR range. The mirror diameter is 3 mm, with a 12.5 cm focal length. The X-ray pulses ionize neon atoms introduced from an effusive nozzle. Photoelectrons are accelerated by the intense laser field according to the instantaneous value of the vector potential at the time of their release [8].

The kinetic energy spectrum of the electrons is recorded using a linear time-of-flight (TOF) spectrometer. The spectrometer consists of a 1 mm hole in an entrance cone, a 60 cm field-free flight tube, and a 25 mm diameter microchannel plate (MCP) detector provided by Jordan TOF Products, Inc. The energy resolution of the TOF is limited by the multichannel scaler used to count electron hits, which has 1 ns bin times. Typical flight times for the fastest electrons are around 250 ns. The solid angle of detection for the TOF spectrometer is determined by the MCP. Typical countrates are on the order of 1–10 electrons per pulse, and a spectrum is typically recorded in 2×10^5 pulses.

For the time-resolved optical streaking measurement, the 730 nm light is filtered out of the central portion of the beam path by a 200 nm thick zirconium filter. The harmonic radiation continues to the inner multilayer mirror while the 730 nm pulse is reflected by an outer annular mirror of 1 inch diameter with a 3.5 mm hole, also coated with the molybdenum/silicon multilayer structure. The temporal delay between the two pulses can be adjusted by moving the inner mirror along the beam axis using a feedback-controlled piezoelectric actuator.

3. HCO analysis

A typical HHG spectrum for the CEP-locked driver pulse is shown in Fig. 3. When the spectrum is Fourier filtered to remove the modulation at twice the laser frequency ($2\omega_L$), broad maxima become discernible. The energies of these maxima correspond to the cutoff energies of the individual half-cycle harmonic emission events [21]. Since the cutoff energy E_{HCO} scales linearly with the time-dependent intensity $I(t)$ of the driving laser (and the target gas ionization potential I_P) via the cutoff law [30,4],

$$E_{HCO} = 3.17U_p + I_P, \tag{1}$$

$$U_p = \frac{I(t)}{4\omega_L^2}, \tag{2}$$

the maxima in the harmonic spectrum also yield information about the time-dependent intensity of the driving pulse during the HHG emission time. Eqs. (1) and (2) are in atomic units.

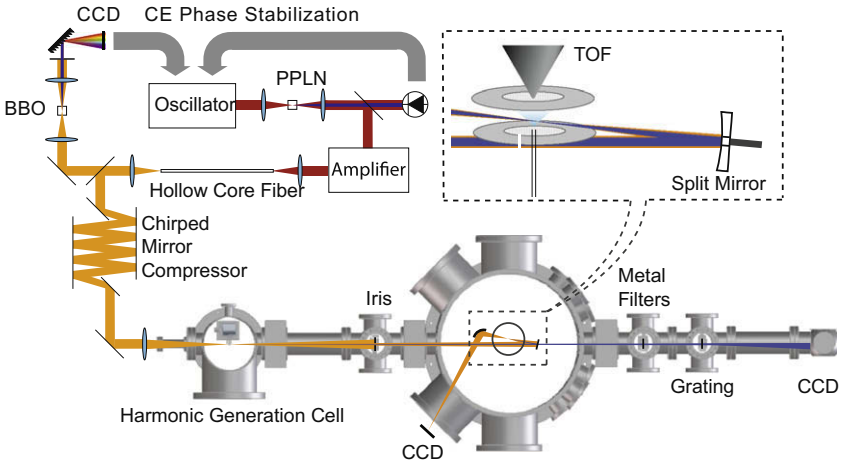

Fig. 2. *Apparatus.* The output of the amplifier is spectrally broadened and temporally recompressed before HHG in the vacuum chamber. In vacuum, an iris varies the amount of 730 nm light reaching the interaction region. A metal filter on a pellicle passes only X-rays on the beam axis, reducing the visible beam to an annular shape. The pulses are focused into the interaction region by a split mirror, the inner portion of which is mounted on a piezoelectric translation stage and reflects the X-rays, while the outer portion reflects the visible light. Photoelectrons generated in the interaction region are analyzed by a time-of-flight detector.

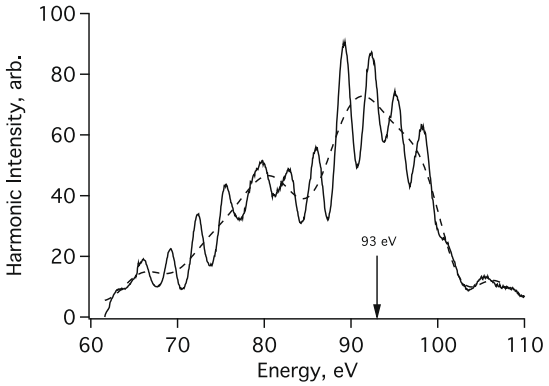

Fig. 3. *Harmonic spectrum* (solid line) and Fourier filtered spectrum (dashed line) at a CEP offset of 0.4π rad showing HCOs at 93 eV and 80 eV.

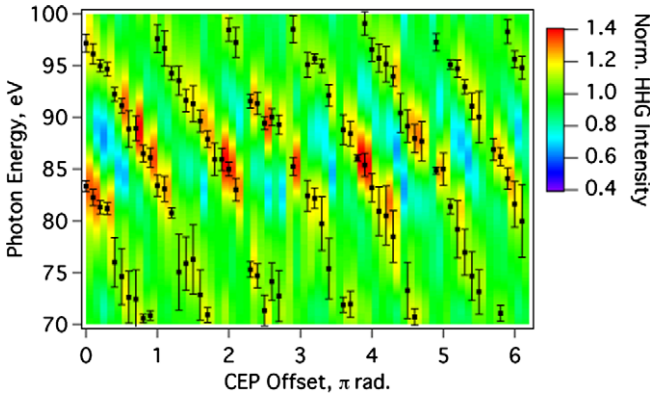

Fig. 4. *Normalized harmonic intensity* versus energy and CEP offset. The $2\omega_L$ modulation is removed by Fourier filtering. Black dots indicate maxima in the spectrum with error bars corresponding to the standard deviation of the HCO positions in the 20 spectra recorded per CEP offset. The linear dependence of the HCO position on CEP is indicative of ionization gating of HHG on the leading edge of the driving pulse.

Collecting many such spectra as a function of the CEP yields the results in Fig. 4. The HCO positions as a function of CEP are marked by black dots. Unfolding the π ambiguity in the data and converting the CEP to a relative time value using the carrier frequency of the laser pulse, the time-dependent intensity of the driver pulse during the harmonic emission is recovered. In Fig. 5, the HCO positions are least-squares fit by an 8 fs half-width Gaussian function with a peak intensity $5.25 \pm 0.10 \times 10^{14}$ W/cm^2. The error estimate on the intensity value is not derived from the least-squares fitting procedure (which yields an artificially small error), but is generated using the ionization gate closure time, as discussed below.

Using the cycle-averaged Ammosov–Delone–Krainov (ADK) ionization rate [31] one can compute the ionization fraction as a function of time. The rate, with all quantities in atomic units, is [32]

$$\eta(t) = \omega_A C_{n^*}^2 f(l,m) I_p \left(\frac{3\epsilon(t)}{\pi(2I_p)^{3/2}}\right)^{1/2} \left(\frac{2(2I_p)^{3/2}}{\epsilon(t)}\right)^{2n^*-|m|-1} \times exp\left(-\frac{2(2I_p)^{3/2}}{3\epsilon(t)}\right) \quad (3)$$

with ω_A the atomic unit of frequency, $\epsilon(t)$ the electric field amplitude, and I_p the ionization potential. The ionization proceeds from states with $l = 1,\ m = 0, \pm 1$ and $n^* = Z \times (2I_p)^{-1/2}$ ($Z = 1$ being the final charge of the ion core). The factors f and C are:

$$f(l,m) = \frac{(2l+1)(l+|m|)!}{2^{|m|}(|m|)!(l-|m|)!} \quad (4)$$

and

$$C_{n^*} = \left(\frac{2e}{n^*}\right)^{n^*} \frac{1}{\sqrt{2\pi n^*}} \quad (5)$$

with e the base of the natural logarithm.

The extent of ionization, determined as a function of time according to Eq. (3), is used to calculate the phase slip between the harmonics and the driving field. This phase slip Δk consists of three terms accounting for the plasma dispersion, the linear dispersion of the generating medium, and the Gouy phase respectively [20]:

$$\Delta k = q k_\omega - k_{q\omega} = P\eta(t) N_{atm} r_e \left(q\lambda - \frac{\lambda}{q}\right) - P\frac{2\pi(1-\eta(t))q}{\lambda}\Delta\delta - (q-1)\frac{\partial}{\partial z}\arctan\left(\frac{z}{z_R}\right). \quad (6)$$

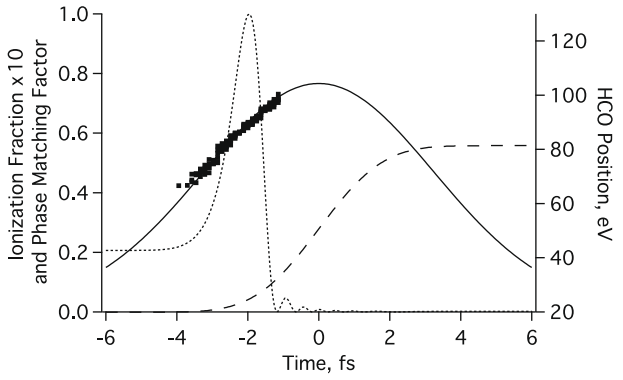

Fig. 5. *HCO positions* (black squares) are fit to an 8 fs Gaussian pulse (solid line) with $5.25 \pm 0.10 \times 10^{14}$ W/cm^2 peak intensity. The ionization fraction (dashed line) calculated by the ADK formula grows to approximately 5% by the end of the pulse. The phase matching factor (dotted line) initially grows then suddenly drops to zero as the ionization fraction exceeds ~1%.

Here, P is the pressure in atmospheres, $\eta(t)$ is the time-dependent ionization fraction, N_{atm} is the number density of one atmosphere, $r_e = 2.82 \times 10^{-15}$ m is the classical electron radius, and λ is the driving field wavelength. The harmonic order is given by q; $\Delta\delta$ is the difference in refractive indices for the driver and harmonic at one atmosphere; z is the gas cell distance from the focus; and z_R is the Rayleigh range, which is the focal spot area divided by the wavelength. The atomic dipole phase [33,20] was neglected for this calculation because its effect on the calculated gate closure time is less than the temporal resolution of the HCO experiment (0.2π rad $\simeq$ 270 as).

Comparing the time resolution of the HCO experiment to the change of t_g with intensity, where t_g is the calculated ionization gate closure time, yields the previously-quoted error estimate of $\pm 0.10 \times 10^{14}$ W/cm^2.

Using Eq. (6), the coherence length is $L_c = \pi/\Delta k$ and the phase matching factor is $F = sinc^2(\pi L/2L_c)$ with L the effective harmonic generation medium length. Here, an effective cell thickness of 3 mm accounting for gas leaking from the holes in the cell, a pressure of 100 mbar, a distance of 11 mm from the focus to the cell, and a Rayleigh range of 9 mm, corresponding to the actual HHG geometry, are employed. As can be seen in Fig. 5, a very rapid loss of phase matching occurs near −1.2 fs, curtailing HHG on the leading edge of the pulse.

At such high intensities and gas densities, both spatial and temporal pulse reshaping are expected to occur. Because the HCO analysis is sensitive to the leading edge of the driving pulse, it cannot reveal distortions that occur later in time.

By tuning the CEP it is possible to spectrally overlap one HCO with the multilayer mirror reflectivity band centered at 93 eV. The HCO energy dependence indicates that this would be possible near a CEP offset of 0.4π rad. However, whether the X-ray emission actually comprises an IAP at this CEP offset is unclear since the recorded raw X-ray spectra are modulated by the spectral overlap of neighboring HCOs (Fig. 3) and do not show a smooth continuum. Nevertheless, an IAP could be anticipated in light of the fact that a hypothetical 10% intensity harmonic prepulse would cause nearly a 40% modulation depth in the spectrum. Techniques to unravel and evaluate temporally separated HCO emission occurring at the same photon energy are presented in the next sections.

4. CEP-scanning

To assess the degree of isolated attosecond pulse production, we employ the technique of CEP-scanning recently introduced by our group in Ref. [29]. CEP-scanning works in the following way. The HCO emission events described in Section 3 come at the zero-crossing times of the driving electric field [34], because they are composed of cutoff harmonics. Since the zero-crossing of the field is a maximum in the vector potential, electrons ionized by the cutoff harmonics (HCOs) receive a large momentum kick in either the upward or downward direction, if the time delay between the harmonic light and the intense streaking field is held at zero (e.g., when both pulses are refocused into the interaction region by the same mirror). Electrons born into the continuum during consecutive half-cycles will receive momentum kicks in opposite directions and therefore the attosecond electron emission from neighboring half-cycles can be observed and compared. This allows measurement of the attosecond pulse contrast as a function of CEP, as illustrated in Fig. 6. Not only can neighboring half-cycle harmonic bursts be compared, but the IAP contrast in the interaction region can be mapped in this way as a function of CEP.

Fig. 7 shows the experimental photoelectron spectrum of neon gas as a function of CEP. The photoelectron signal, which would come near 70 eV in the absence of a streaking field, splits into two components, one higher and one lower in energy. With only

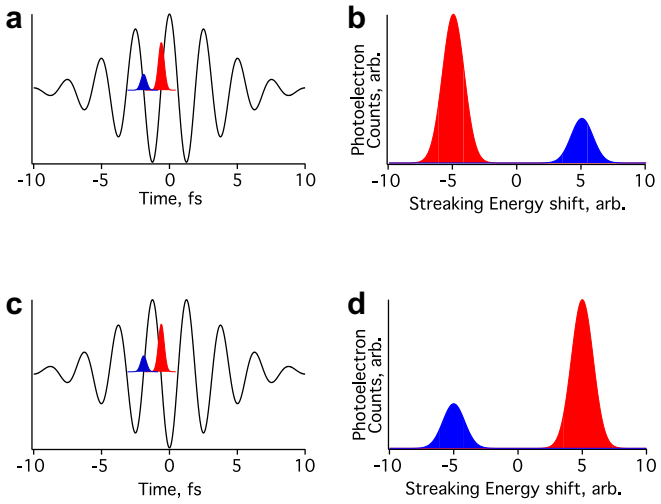

Fig. 6. *Principle of the CEP-scanning method* for attosecond pulse contrast retrieval. Using the vector potential of the driving laser to alter the photoelectron momentum enables separation of ionization events in the main X-ray pulse from satellites spaced half an optical cycle earlier or later. Comparing the "up-streaked" (or "down-streaked") photoelectron signal before (panels a and b) and after (panels c and d) changing the CEP by π enables direct contrast retrieval. Alternatively, the up-streaked and down-streaked peaks may be compared directly at fixed CEP.

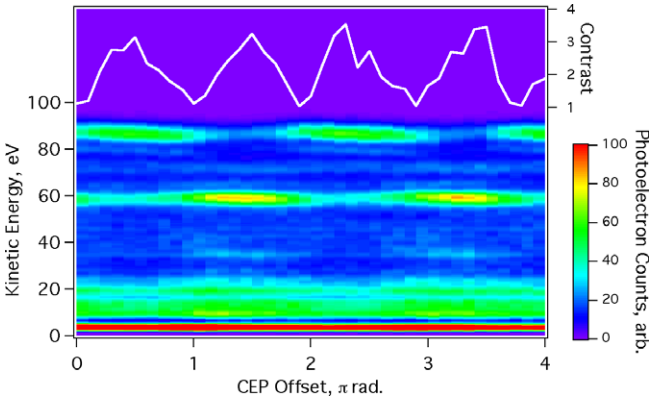

Fig. 7. *CEP-dependent photoelectron spectrum* of Ne at zero time delay between the X-ray bursts and the streaking field. The attosecond pulse contrast (white line) is retrieved from the CEP-dependent intensity of the peaks near 60 eV and 90 eV.

two CEP-dependent peaks in the photoelectron spectrum, the contrast can be measured between a central pulse and up to two satellite pulses spaced single half-cycles away in time. Subtracting a linear background over the analyzed energy range and then comparing the up-streaked peak area between CEP values separated by π yields $c = 3.3 \pm 0.2$ (average ± standard deviation of the four contrast maxima shown in the white line in Fig. 7) for the optimal CEP offset value of 0.5π rad. The same result is obtained by comparing the two peak areas at fixed CEP offset. The CEP offset value maximizing c is slightly different from the value anticipated from the HCO analysis because some harmonic flux from multiple half-cycles of the driving pulse, not just the one producing an HCO centered at 93 eV, reflects off the multilayer mirror and needs to be accounted for.

We emphasize that although this contrast measurement scheme is limited to comparing one main IAP to neighboring pulses that are offset by half an optical cycle, it is general to all methods of IAP generation that depend on the CEP.

5. Optical streaking

Finally, we use time-resolved optical streaking [8] with the split-mirror configuration described in Section 2 to confirm that ionization gating produces isolated attosecond pulses. A sufficiently well-resolved spectrogram (photoelectron spectrum versus time delay) contains enough information for the full determination of both the HHG and driver pulse shapes [35]. The experimental time-resolved photoelectron spectrum of neon atoms is shown in Fig. 8 as a function of infrared pulse time delay. Visually, one can observe the individual half-cycles of the driving electric field, which alternately accelerate the attosecond photoelectron wavepacket upwards and downwards. The white arrows separated by the optical period (2.4 fs) mark the full-optical-cycle periodicity in the photoelectron streaking, which would be averaged over in the case of an X-ray pulse longer than the half-cycle time.

The spectrogram can be fit using a Monte Carlo method in which suitably parametrized XUV and infrared pulses are chosen at random, a trial spectrogram is calculated and blurred according to the instrumental resolution, and the result compared to the experiment. If the mean squared error (MSE) is reduced with respect to the previous best fit, the current guess is taken as the new best fit. An adjustable numerical "temperature" enables the best fit to be updated (with Boltzmann probability) to a guess with a larger value of MSE. The initial parameters are chosen by hand in an effort to minimize the starting MSE, and the step size in any direction in parameter space is limited to be less than ±5% the initial parameter value corresponding to that direction.

There are drawbacks to the Monte Carlo method, including significantly slower convergence than FROG-CRAB [35,36]. Further, the method can be very insensitive to a certain pulse parameter if the gradient of the MSE function in that direction of parameter space is small. In this case, a different parameterization of the pulses is required. However, for noisy data sets our technique has the advantage over the FROG-CRAB method that the number of parameters is reduced from hundreds to a handful (on the order of 10). This strongly restrains the program from attempting to match noise by guessing an extremely complicated vector potential, a common problem we have experienced using FROG-CRAB on noisy data sets.

The attosecond pulse contrast is fixed at the previously-measured value of 3.3, and the carrier frequency is fixed at 2.35 fs^{-1}. The retrieved attosecond pulse duration is 430 ± 15 as, roughly consistent with the 450 as bandwidth limit for reflection off the 4 eV bandwidth XUV mirror. That the pulses delivered to the interaction region are nearly transform limited is a result of their position at the cutoff of the HHG spectrum, where the temporal phase has (to a first approximation) no quadratic component [34].

The vector potential of the driving pulse is also retrieved, which corresponds to a 7 fs Gaussian intensity profile with a small prepulse, consistent with the HCO measurement. Pre- and postpulses commonly accompany ultrashort pulses because of the difficulty in producing and phase-compensating ultra-broad-bandwidth laser sources, but the measured prepulse is not intense enough to ionize the harmonic generation medium and so it does not produce harmonics or contribute toward the critical ionization threshold discussed in Section 3.

The time-dependent streaking results not only confirm the conclusions of the previous sections, but also illustrate some interesting points about the ionization-gating regime of HHG. The closure of the ionization gate relies on an ultrafast loss of phase matching. Isolated attosecond pulse production is an indication that the index of refraction of the target gas can change on the attosecond timescale, a surprisingly fast time for changes in a *macroscopic* property. Furthermore, the results demonstrate that the idea of an unmodulated X-ray continuum being required for useful isolated attosecond pulses is overly cautious. In fact, a very small X-ray satellite pulse can lead to a large modulation depth in the spectrum, and this fact speaks to the need for temporal characterization techniques to determine the structure of attosecond X-ray fields. Besides the time-resolved streaking shown in this section, the CEP-scan is an extremely useful and fast way to accomplish this.

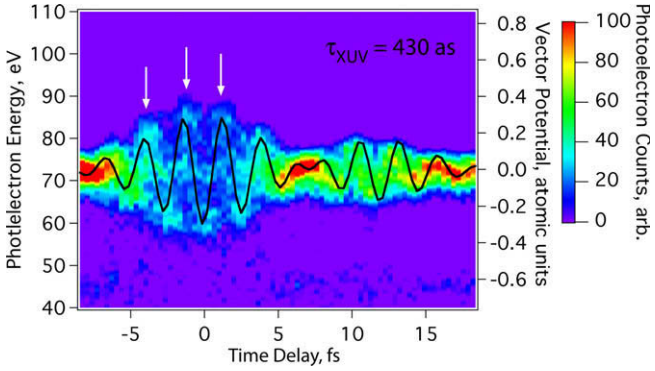

Fig. 8. *Streaking spectrogram* showing the isolated nature of the attosecond pulse. The streaked photoelectron spectrum, shown versus infrared pulse delay time, reveals the duration of the XUV pulse to be 430 ± 15 as. It also reveals the vector potential of the infrared pulse, shown by the black line, which is a 7 fs Gaussian shape with a prepulse.

6. Conclusion

Ionization gating of HHG emission is shown to produce isolated attosecond pulses with variable, CEP-dependent contrast. The ionization gate is perhaps the most explicit example so far of the *selection* (rather than simply *generation*) of an attosecond pulse by a combination of microscopic and macroscopic factors, as discussed by Gaarde and co-workers [37].

The isolated nature of the pulse is characterized with the newly developed method of CEP-scanning and confirmed by time-resolved optical streaking. Since the ionization gating scheme is scalable to longer, multicycle driver pulses, we anticipate that IAP production is also achievable using long pulses. Indeed, an interesting step in that direction has recently been achieved in Ref. [38], where sub-femtosecond pulses were demonstrated using 15 fs drivers without carrier–envelope phase stabilization. By implementing ionization gating with such driver pulses with CEP stabilization, isolated tunable attosecond pulses with no timing jitter

with respect to the driver laser intensity envelope (as occurs without CEP stabilization) can be generated without the need to resort to more complicated schemes involving multiple colors or polarization control.

Acknowledgements

The authors wish to thank Lukas Gallmann, Jason Jones, and Jun Ye for significant contributions to the experimental apparatus. We also thank Andrew Aquila, Yanwei Liu, Michael Hofstetter, and Ulf Kleineberg for manufacturing the multilayer X-ray mirrors. The project is supported by a MURI program from the Air Force Office of Scientific Research, Contract No. FA9550-04-1-0242. Portions of the laboratory were supported by the Director, Office of Science, Office of Basic Energy Sciences, of the US Department of Energy under Contract DE-AC02-05CH11231. T.P. acknowledges support of a Feodor Lynen Fellowship of the Alexander von Humboldt-Foundation. M.J.B. and P.M.N. are recently supported by a National Science Foundation Chemistry grant. Stephen Leone gratefully acknowledges the generous support of a Morris Belkin Visiting Professorship at the Weizmann Institute of Science.

References

[1] M. Drescher, M. Hentschel, R. Kienberger, M. Uiberacker, V. Yakovlev, A. Scrinzi, T. Westerwalbesloh, U. Kleineberg, U. Heinzmann, F. Krausz, Nature 419 (2002) 803.
[2] T. Pfeifer, M.J. Abel, P.M. Nagel, A. Jullien, Z.-H. Loh, M.J. Bell, D.M. Neumark, S.R. Leone, Chem. Phys. Lett. 463 (2008) 11.
[3] A. Cavalieri, N. Muller, T. Uphues, V. Yakovlev, A. Balthuška, B. Hovrath, B. Schmidt, L. Blumel, R. Holzwarth, S. Hendel, M. Drescher, U. Kleineberg, P. Echenique, R. Kienberger, F. Krausz, U. Heinzmann, Nature 449 (2007) 1029.
[4] P.B. Corkum, Phys. Rev. Lett. 71 (1993) 1994.
[5] E. Cormier, P. Lambropolous, Eur. Phys. J. D 2 (1998) 15.
[6] T. Nakajima, E. Cormier, Opt. Lett. 32 (2007) 2879.
[7] M.J. Abel, T. Pfeifer, A. Jullien, P.M. Nagel, M.J. Bell, D.M. Neumark, S.R. Leone, J. Phys. B: At. Mol. Opt. Phys. 42 (2009) 075601.
[8] R. Kienberger, E. Goulielmakis, M. Uiberacker, A. Baltuška, V. Yakovlev, F. Bammer, A. Scrinzi, T. Westerwalbesloh, U. Kleineberg, U. Heinzmann, M. Drescher, F. Krausz, Nature 427 (2004) 817.
[9] D. Lappas, A. L'Huillier, Phys. Rev. A: At. Mol. Opt. Phys. 58 (1998) 4140.
[10] G. Sansone, E. Benedetti, F. Calegari, C. Vozzi, L. Avaldi, R. Flammini, L. Poletto, P. Villoresi, C. Altucci, R. Velotta, S. Stagira, S.D. Silvestri, M. Nisoli, Science 314 (2006) 443.
[11] T. Pfeifer, L. Gallmann, M.J. Abel, D.M. Neumark, S.R. Leone, Opt. Lett. 31 (2006) 975.
[12] T. Pfeifer, L. Gallmann, M.J. Abel, P.M. Nagel, D.M. Neumark, S.R. Leone, Phys. Rev. Lett. 97 (2006) 163901.
[13] H. Xiong, R. Li, Z. Zeng, Y. Zheng, Y. Peng, X. Yang, X. Chen, H. Zeng, Z. Xu, Phys. Rev. A: At. Mol. Opt. Phys. 75 (2007) 051802.
[14] Y. Zheng, Z. Zeng, X. Li, X. Chen, P. Liu, H. Xiong, H. Lu, S. Zhao, P. Wei, L. Zhang, Z. Wang, J. Liu, Y. Cheng, R. Li, Z. Xu, Opt. Lett. 33 (2008) 234.
[15] L. Zheng, S. Tang, X. Chen, Opt. Express 17 (2009) 538.
[16] Z. Chang, Phys. Rev. A: At. Mol. Opt. Phys. 71 (2005) 023813.
[17] Z. Chang, Phys. Rev. A: At. Mol. Opt. Phys. 76 (2007) 051403.
[18] T. Pfeifer, A. Jullien, M.J. Abel, P.M. Nagel, L. Gallmann, D.M. Neumark, S.R. Leone, Opt. Express 15 (2007) 17120.
[19] A. Jullien, T. Pfeifer, M.J. Abel, P.M. Nagel, M.J. Bell, D.M. Neumark, S.R. Leone, Appl. Phys. B 93 (2008) 433.
[20] A. Paul, E. Gibson, X. Zhang, A. Lytle, T. Popmintchev, X. Zhou, M. Murnane, I. Christov, H. Kapteyn, IEEE J. Quantum Electron. 42 (2006) 14.
[21] C.A. Haworth, L.E. Chipperfield, J.S. Robinson, P.L. Knight, J.P. Marangos, J.W.G. Tisch, Nat. Phys. 3 (2007) 52.
[22] J. Reichert, R. Holzwarth, T. Udem, T. Hänsch, Opt. Commun. 172 (1999) 59.
[23] H.R. Telle, G. Steinmeyer, A.E. Dunlop, J. Stenger, D.H. Sutter, U. Keller, Appl. Phys. B 69 (1999) 327.
[24] D.J. Jones, S.A. Diddams, J.K. Ranka, A. Stentz, R.S. Windeler, J.L. Hall, S.T. Cundiff, Science 288 (2000) 635.
[25] M. Nisoli, S.D. Silvestri, O. Svelto, Appl. Phys. Lett. 68 (1996) 2793.
[26] M. Nisoli, S.D. Silvestri, O. Svelto, R. Szipöcs, K. Ferencz, C. Spielmann, S. Sartania, F. Krausz, Opt. Lett. 22 (1997) 522.
[27] L. Gallmann, T. Pfeifer, P.M. Nagel, M.J. Abel, D.M. Neumark, S.R. Leone, Appl. Phys. B 86 (2007) 561.
[28] A. Baltuška, M. Uiberacker, E. Goulielmakis, R. Kienberger, V. Yakovlev, T. Udem, T. Hansch, F. Krausz, IEEE J. Sel. Top. Quantum Electron. 9 (2003) 972.
[29] T. Pfeifer, M.J. Abel, P.M. Nagel, W.F. Boutu, M.J. Bell, Y. Liu, D.M. Neumark, S.R. Leone, Opt. Lett. 34 (2009) 1819.
[30] J. Krause, K. Schafer, K. Kulander, Phys. Rev. Lett. 68 (1992) 3535.
[31] M.V. Ammosov, N.B. Delone, V.P. Krainov, Sov. Phys. JETP 64 (1986) 1191.
[32] S. Augst, D.D. Meyerhofer, D. Strickland, S.L. Chin, J. Opt. Soc. Am. B 8 (1991) 858.
[33] M. Lewenstein, P. Salières, A. L'huillier, Phys. Rev. A 52 (6) (1995) 4747.
[34] Y. Mairesse, A. de Bohan, L. Frasinski, H. Merdji, L. Dinu, P. Monchicourt, P. Breger, M. Kovacev, T. Auguste, B. Carré, Phys. Rev. Lett. 93 (2004) 163901.
[35] Y. Mairesse, F. Quéré, Phys. Rev. A: At. Mol. Opt. Phys. 71 (2005) 1.
[36] J. Gagnon, E. Goulielmakis, V.S. Yakovlev, Appl. Phys. B 92 (2008) 25.
[37] M.B. Gaarde, J.L. Tate, K.J. Schafer, J. Phys. B: At. Mol. Opt. Phys. 41 (2008) 132001.
[38] I. Thomann, A. Bahabad, X. Liu, R. Trebino, M. Murnane, H. Kapteyn, Opt. Express 17 (2009) 4611.